EuroGNC Navigation Guidance Control CEAS Bristol, UK June 11th-13th 2024
University of BRISTOL ROYAL AERONAUTICAL SOCIETY AIAA

De-orbit Trajectory Design for Reusable Unmanned Space Vehicle using Sequential Convex Optimization with Multiple Re-Entry Targets

Jaewon Kim M.S. candidate, Seoul National University, Department of Aerospace Engineering, 08826, Seoul, Republic of Korea. vgkjw@snu.ac.kr

Sangmin Lee Ph.D. candidate, Seoul National University, Department of Aerospace Engineering, 08826, Seoul, Republic of Korea. everlastingminii@gmail.com

Youdan Kim Professor, Seoul National University, Department of Aerospace Engineering, 08826, Seoul, Republic of Korea. ydkim@snu.ac.kr

Chandeok Park Associate Professor, Yonsei University, Department of Astronomy, 03722, Seoul, Republic of Korea. park.chandeok@yonsei.ac.kr

ABSTRACT

As new space missions requiring rapid response and the ability to achieve multiple objectives within a single mission are taking attention, the need for reusable spacecraft capable of handling diverse tasks is increasing. In this study, the trajectory generation problem for de-orbit missions with multiple re-entry targets is considered using convex optimization methods, focusing on the application of Reusable Unmanned Space Vehicles(ReUSVs). The nonlinear de-orbit trajectory generation problem is formulated from the initial mission orbit to the final re-entry target with specific re-entry constraints. Then, the formulated problem is convexified, and the sequential convex programming method is used to solve the multiple de-orbit trajectory optimization problem. Numerical simulation shows that the proposed methods can generate multiple de-orbit trajectories efficiently, which demonstrates the effectiveness of convex optimization for generating trajectories even in the presence of uncertainties.

Keywords: Reusable Unmanned Space Vehicle (ReUSV); Sequential Convex Optimization; De-Orbit Phase; Entry Target Selection

Nomenclature

μ	=	Gravitational Constant
r	=	radial distance
θ	=	azimuth angle
ϕ	=	elevation angle
v_r	=	radial direction velocity
v_θ	=	azimuth angle direction velocity
v_ϕ	=	elevation angle direction velocity
m	=	mass

T = Thrust

1 Introduction

As the New Space Era begins, various types of new space missions such as debris removal, surveillance, and space reconnaissance have received a lot of attention. Conventional spacecraft, which are usually designed to perform a specific single mission, have some limitations in dealing with these complicated missions. Thus, there is a growing need for Reusable Unmanned Space Vehicles (ReUSVs) that can perform various missions with high reusability and accuracy. ReUSVs are particularly effective for composite missions that require swift responses or multiple objectives within a single launch. Considering these aspects, the trajectory generation algorithm of ReUSVs must be developed to achieve multiple objectives while satisfying various constraints required for preserving the reusability of ReUSVs.

Generally, the mission phases of a ReUSV can be segmented into the Ascent phase, On-orbit phase, De-orbit phase, and Re-entry phase. The Ascent phase begins with the launch and involves inserting the vehicle into the orbit where the primary mission will be performed. The "On-orbit phase" collectively refers to the segment where the Reusable Launch Vehicle (RLV) achieves either a single or multiple mission objectives after the launch.

Once the given objectives of the vehicle are achieved, the vehicle should leave the orbit to return to the Earth by passing through the segment called the de-orbit phase before entering the atmosphere. The Re-entry phase begins with entering the atmosphere, which involves dissipating the mechanical energy until the vehicle reaches the landing site [1]. To successfully perform the Re-entry phase, the de-orbit phase should be completed by satisfying several constraints referred to as entry interface (EI) conditions in a specified area called the Re-entry boundary, at an altitude of about 120 km [2][3].

Research on the de-orbit phase has not been done much compared to other mission phases, because the operation time of the de-orbit phase is short and the requirement imposed on the de-orbit phase is relatively mild in many missions [4]. However, in designing the ReUSV mission trajectory where maximizing reusability is essential, the ReUSV is required to complete the de-orbit phase satisfying the EI conditions accurately. Therefore, a trajectory generation method specialized for the de-orbit phase of ReUSV should be developed.

Typically, impulsive thrust is applied to perform de-orbit. De-orbit, when not considering some constraints involving final time and load, generates a trajectory similar to the problem of orbit transfer. Therefore, it can be simplified to a 2-body problem and can be solved by an analytic method, creating a minimum ΔV de-orbit trajectory similar to the Hohmann transfer [4]. However, this method does not take into account perturbations such as the J2 effect and does not offer robust guidance under the influence of irregular environments such as solar winds. Hence, to consider more complicated dynamics, solutions to the minimum-impulse de-orbit problem can be derived using direct optimization [5], multiple-shooting method [6], and primer vector theory [7]. De-orbit using impulsive thrust has advantages with considering relations between each input or state and the trajectory, which is effective in obtaining the intended re-entry point. However, because it does not employ continuous thrust, achieving de-orbit at the intersection of the mission orbit plane and the re-entry point requires either maintaining the orbit and waiting until a suitable relative position is met, or performing an additional phasing maneuver, to forcibly achieve the required relative position [8].

To overcome such limitations, several studies have been conducted using continuous thrust for de-orbit or orbit transfer. Similar to the impulsive thrust case, the indirect shooting method was used to resolve orbit transfer problems [9], and direct control parameterization was used [10]. In the case of research on continuous thrust-optimal trajectory generation using parametric optimization, 6-th degree

inverse polynomial was employed for a shape-based approach to generate minimum fuel optimal trajectory [11] and Fourier series-based shape-based method was used for similar problems [12].

Recently, in the field of aerospace engineering, methodologies employing convex optimization have been actively studied for various problems to obtain the solution efficiently. Typically, for general space missions, trajectories are designed based on thorough planning offline, and the execution adheres as closely as possible to the completed plan in online situations [13]. However, as discussed previously, swift task execution and completion are crucial for missions requiring ReUSV, thus generating robust and feasible solutions in on-board situations is becoming increasingly important. In this study, sequential convex optimization is employed to generate a de-orbit trajectory considering the uncertainties in the landing point of ReUSV's mission. The main contribution of this study is to demonstrate the effectiveness of convex optimization in ReUSV's space missions.

This paper is organized as follows: In Section 2, the problem considered in this study is formulated as the optimization problem. In Section 3, convexification of the problem formalized in Section II is performed for sequential convex optimization, In Section 4, a decision algorithm using sequential convex optimization techniques is presented for the uncertain Landing point. In Section 5, the proposed techniques are applied to cases with single or multiple Landing points. Finally, in Section 6, the conclusion is given.

2 Problem Formulation

This section formulates the trajectory generation problem for the deorbit problem which begins at 'Mission orbit' and ends at 'Re-entry target'. Then, the formulated problem is modified by convexifying the objective function and constraints, making it suitable for the application of the Successive Convexification Programming (SCP) algorithm. Typically, the mission of a Reusable Launch Vehicle (RLV) can be divided into the Ascent phase, On-orbit phase, De-orbit phase, and Re-entry phase. During the Ascent phase, the vehicle is launched and ascends its altitude to the orbit where the main mission is to be executed. During the On-orbit phase, the RLV performs its single or multiple missions. After achieving its goals, the stage leading up to entry into the atmosphere from the mission-performing orbit is called the De-orbit phase. Subsequently, the process of depleting the remaining kinetic energy after entering the atmosphere and reaching the Landing point is termed as Re-entry phase. It is known that, to successfully execute the Re-entry phase, the De-orbit phase must be completed in a specified region at an altitude of 120km centered around the Landing point, which is called Re-entry boundary [2].

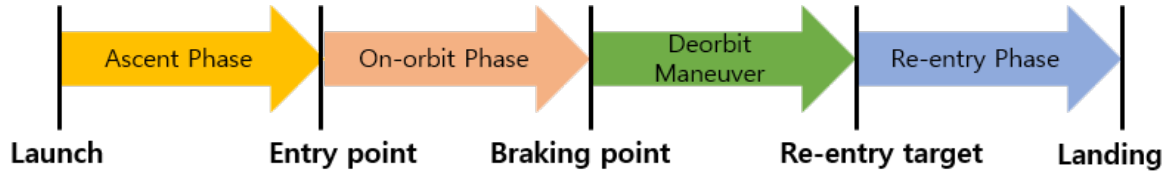

Fig. 1 RLV mission phase division

In this study, the optimal control problem of directing an RLV is considered, where the RLV operates at an altitude of 400km in Low Earth Orbit (LEO) to perform a de-orbit maneuver from an arbitrary braking point and to reach a designated re-entry target at an altitude of 120km, while maintaining the specified attitude. Based on the problem formulated in this section, the SCP algorithm is applied to generate the de-orbit trajectory and solve the real-time path generation and selection problem for multiple re-entry targets.

2.1 Equations of Motions

Compared to other mission phases of the Reusable Launch Vehicle (RLV), the de-orbit phase is typically short in duration and occurs at altitudes above 120km. Therefore, it is reasonable to neglect the perturbations due to aerodynamics [4]. Based on the conventional 2-body equation in spherical coordinates considering the RLV as a point mass, the equations of motion for the de-orbit maneuver of the ReUSV are given as follows [14].

$$
\begin{aligned}
\dot{r} &= v_r \\
\dot{\theta} &= \frac{v_\theta}{r cos\phi} \\
\dot{\phi} &= \frac{v_\phi}{r} \\
\dot{v_r} &= \frac{v_\theta^2 + v_\psi^2}{r} - \frac{\mu}{r^2} + \frac{T_r}{m} \\
\dot{v_\theta} &= -\frac{v_r v_\theta}{r} + \frac{v_\theta v_\phi \tan\phi}{r} + \frac{T_\theta}{m} \\
\dot{v_\phi} &= -\frac{v_r v_\phi}{r} - \frac{v_\theta^2 \tan\phi}{r} + \frac{T_\phi}{m} \\
\dot{m} &= -\frac{T}{v_e}
\end{aligned}
\tag{1}
$$

where r represents the radial distance from the center of Earth to the ReUSV, θ represents the azimuth angle, ϕ represents the elevation angle, m represents the mass of the spacecraft, and μ is the gravitational constant of Earth. The terms v_r, v_θ, and v_θ correspond to the velocities in the radial, azimuthal, and elevation directions, respectively. The exhaust velocity, v_e, is defined by $I_{sp}g_0$. T is the thrust magnitude, and T_r, T_θ, and T_ϕ represent the components of the thrust in the r, θ, and ϕ direction, respectively, and each term represents the directional cosine components of T. Therefore, the following constraints should be imposed on the control variables.

$$
T_r^2 + T_\theta^2 + T_\phi^2 = T^2,\ T \geq 0 \tag{2}
$$

The state variable is represented as $\mathbf{x} = [r, \theta, \phi, v_r, v_\theta, v_\phi, m]$, and the control variable is represented as $\mathbf{u} = [T_r, T_\theta, T_\phi, T]$. The propulsion system used for this study is a bipropellant, single aerojet engine which is modeled based on the X-37B's thruster.

2.2 Constraints

The initial state of the RLV maneuver corresponds to the state at the instance of the de-orbit, which is determined by the mission design of the on-orbit. The terminal state is constrained to be inside the re-entry boundary, which can be derived by appropriate mathematical techniques to make the RLV reach a predetermined landing point on the Earth [15]. Consequently, the terminal coordinates required to be met at the starting altitude of re-entry, 120km, are determined. The terminal flight path angle is constrained within certain limits to manage the heat load and normal and axial loads experienced during atmospheric entry.

The initial conditions are denoted as follows:

$$
\mathbf{x}(t_0) = [r(t_0), \theta(t_0), \phi(t_0), v_r(t_0), v_\theta(t_0), v_\phi(t_0), m(t_0)] \tag{3}
$$

The terminal conditions derived from the pre-specified re-entry target are denoted as follows:

$$\mathbf{x}(t_f) = [r(t_f), \theta(t_f), \phi(t_f)] \tag{4}$$

In addition, the terminal flight angle is constrained as follows:

$$\gamma(t_f) = -3.0^\circ \tag{5}$$

which can be reformulated as :

$$\arcsin\left(\frac{v_r(t_f)}{\sqrt{v_r(t_f)^2 + v_\theta(t_f)^2 + v_\phi(t_f)^2}}\right) = -3.0^\circ \tag{6}$$

2.3 Dynamic Optimization Problem

The RLV considered in this study is assumed to be a multi-purpose spacecraft, particularly for conducting space missions that are challenging for satellites. Therefore, fuel consumption is important for enhancing the mission capabilities. Solving enough fuel after the de-orbit maneuver is critical for achieving a stable landing if the ReUSV employs a retro-propulsion landing. Therefore, the objective of the optimization is set as minimizing the fuel consumption in this study. The following inequality constraints are also applied to each state and control variables :

$$\begin{aligned} \mathbf{x}_{min} \leq \mathbf{x} \leq \mathbf{x}_{max} \\ \mathbf{u}_{min} \leq \mathbf{u} \leq \mathbf{u}_{max} \end{aligned} \tag{7}$$

where x_{min} and x_{max} denote the lower and upper bounds of the state, respectively, and u_{min} and u_{max} denote the lower and upper bounds of the control variables, respectively.

For r and θ, the bounds are defined to improve the efficiency of the optimum search. The bound for ϕ is imposed according to the range defined by the spherical coordinate representation. For m, the dry mass and initial mass are applied as the bound. The variables $v_r, v_\theta, v_\phi, T_r, T_\theta, T_\phi$ have constraints set to represent the normalized physical values of the spacecraft. By combining the previously derived nonlinear dynamics and constraints, the following constrained optimal control problem can be formulated:

$$\begin{aligned} &\min J = -m(t_f) \\ &\text{subject to : Eqs.}(1) - (4), \text{and } (6) - (7) \end{aligned} \tag{8}$$

3 Sequential Convex Programming Algorithm

3.1 Normalization and Convexification

Normalization is performed on each variable to prevent numerical issues that may arise from the different magnitude of the order of each variable. For r, normalization is done with $R_0 = 6,378km$ where R_0 is the radius of the Earth. For $v_r, v_\theta, v_\phi, v_e$, normalization is done with $V_0 = \sqrt{\frac{\mu}{R_0}}$ where μ is

the gravitational constant of the Earth. Time t is normalized with $\frac{R_0}{V_0}$, mass m with the initial mass m_0, and thrust T with the maximum thrust T_{max} [1].

The optimization problem (8) is characterized by the nonlinear dynamic equation, which includes nonconvex constraints. For the trajectory generation method that can be used in the context of various missions, it is important to reduce the computational load required for generating the trajectory. Therefore, the original optimization problem (8) is convexified as a new problem, and a sequential convex programming algorithm is applied. Based on the methodologies presented in [1], new variables are introduced as :

$$\begin{aligned} \tau &= \frac{T}{m} \\ \tau_r &= \frac{T_r}{m},\ \tau_\theta = \frac{T_\theta}{m},\ \tau_\phi = \frac{T_\phi}{m} \end{aligned} \tag{9}$$

$$z = \ln m \tag{10}$$

Accordingly, the state and control variables are redefined as:

$$\begin{aligned} \hat{\mathbf{x}} &= [r, \theta, \phi, v_r, v_\theta, v_\phi, z]^T \\ \hat{\mathbf{u}} &= [\tau_r, \tau_\theta, \tau_\phi, \tau]^T \end{aligned} \tag{11}$$

with the corresponding constraints

$$\begin{aligned} \hat{\mathbf{x}}_{min} \leq \hat{\mathbf{x}} \leq \hat{\mathbf{x}}_{max} \\ \hat{\mathbf{u}}_{min} \leq \hat{\mathbf{u}} \leq \hat{\mathbf{u}}_{max} \end{aligned} \tag{12}$$

The thrust magnitude constraint (2) and a constraint arising from the change of variables are convexified as

$$\tau_r^2 + \tau_\theta^2 + \tau_\phi^2 \leq \tau^2 \tag{13}$$

$$0 \leq \tau \leq e^{-z_*}[1 - (z - z_*)] \tag{14}$$

The dynamics can be linearized with respect to a reference state trajectory as

$$\dot{\hat{\mathbf{x}}} = f(\hat{\mathbf{x}}_*) + A(\hat{\mathbf{x}}_*)(\hat{\mathbf{x}} - \hat{\mathbf{x}}_*) + B\hat{\mathbf{u}} \tag{15}$$

The detailed expressions of A and B are presented in the Appendix.

Considering linearized dynamics, the errors may occur due to artificial unboundness caused by the difference between the linearized dynamics and the actual dynamics. To prevent this, trust region constraint should be applied [16] :

$$\begin{aligned} ||\hat{\mathbf{x}} - \hat{\mathbf{x}}^k|| \leq \eta_x \\ ||\hat{\mathbf{u}} - \hat{\mathbf{u}}^k|| \leq \eta_u \end{aligned} \tag{16}$$

Then, a convex optimization problem can be defined as the following

$$\begin{aligned} &J = -m(t_f) \\ &\text{subject to : Eqs.}(3) - (6), \text{and } (12) - (15) \end{aligned} \tag{17}$$

Now, sequential convex programming can be used to obtain the optimal trajectory.

3.2 Algorithm

In this section, the convex optimization problem of (17) is considered to obtain the solution, which will be determined by setting the solution trajectory from each iteration as the reference state trajectory for the subsequent iteration. The algorithm is summarized as Algorithm 1:

Algorithm 1 Successive convexification algorithm

Step 1: Generate the initial guess trajectory $\hat{\mathbf{x}}^0(t)$,$\hat{\mathbf{u}}^0(t)$, set $k = 1$
Step 2: Solve the convexified problem P1 using $\hat{\mathbf{x}}^{k-1}(t)$,$\hat{\mathbf{u}}^{k-1}(t)$ as the reference trajectory
Step 3: Update the trust region radius, $k \leftarrow k + 1$
Step 4: repeat step2-step3 until the convergence criterion is met.

First, using the given initial states (3) and a suitable initial control, the initial reference trajectory, $\hat{\mathbf{x}}^{\mathbf{0}}(t)$ and $\hat{\mathbf{u}}^0(t)$ is generated. Second, the convexified linear optimal control problem for the k-th iteration is solved. Here, $\hat{\mathbf{x}}^{(\mathbf{k-1})}$ denotes the optimal state trajectory derived from the previous iteration. Third, after solving the k-th convexified problem, the trust region radius is updated according to the method described in [1]. Finally, for each iteration, if the convergence criterion (18), which is selected considering normalized values, is met, the process terminates. If not, the next step to conduct the $(k + 1)$-th iteration is performed.

$$\sup_{t_0 \le t \le t_f} ||\hat{\mathbf{x}}^{(k)} - \hat{\mathbf{x}}^{(k-1)}|| \le \epsilon, \ k \ge 1 \tag{18}$$

4 Re-entry Target Selection

For the RLV to maximize its mission capabilities, the trajectory from the mission orbit to the landing point should be generated efficiently and reliably. If multiple feasible landing points are available, the point that best aligns with their objectives should be selected. Therefore, trajectories are generated for multiple re-entry targets, choosing the one whose performance index aligns most appropriately.

The convex optimization problem (17) formulated in section 3 is a problem that generates feasible solutions for a single re-entry target. If multiple landing point candidates are viable, then re-entry boundaries can be predetermined for each candidate [15]. Labeling these as $\mathbf{x_1}(t_f)$, $\mathbf{x_2}(t_f)$, ... , $\mathbf{x_i}(t_f)$, $\mathbf{x_n}(t_f)$, a suitable re-entry target can be selected by solving convex optimization problem for each and comparing the performance index, thereby configuring a single-variable optimization in an outer-loop.

$$\mathbf{x}(t_f) \in \left\{\mathbf{x_1}(t_f), \mathbf{x_2}(t_f), ..., \mathbf{x_i}(t_f), ..., \mathbf{x_n}(t_f)\right\} \tag{19}$$

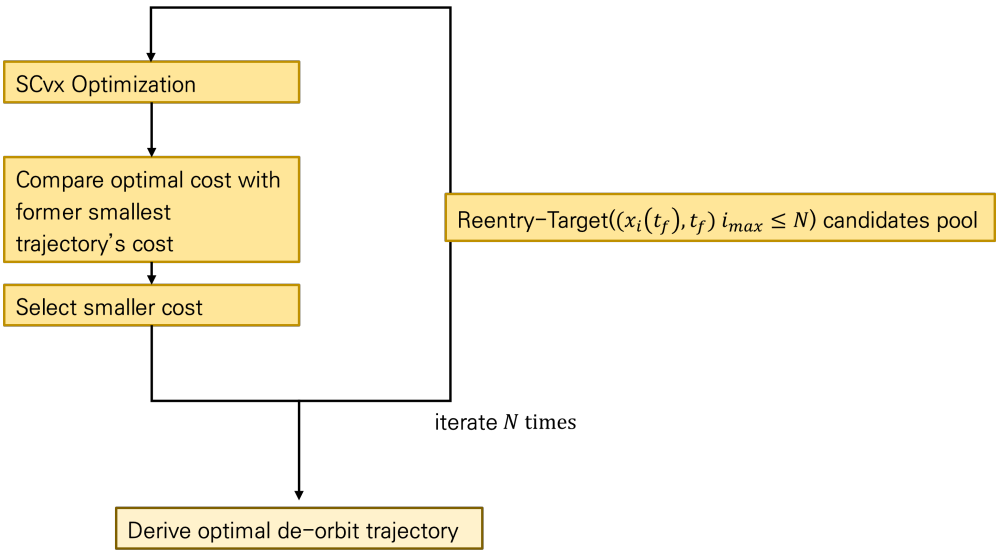

Fig. 2 Re-entry target selection flowchart

Figure 2 shows the re-entry target selection routine.

5 Numerical Simulation

Numerical simulation is performed to demonstrate the effectiveness of the proposed algorithm, which generates de-orbit trajectories using convex optimization. The parameters used for the problem are summarized in Table 1. Parameters related to the propulsion system are selected based on the X-37B engine model, which is considered as R-42.

Parameters	value
Gravitational constant of Earth μ	$3.986012\times10^{14}(m^3/s^2)$
Earth radius R_0	6,378(km)
Initial mass m_0	5,000(kg)
Dry mass m_{dry}	4,000(kg)
Maximum thrust T_{max}	900(N)
Specific impulse I_{sp}	305(s)
Convergence criterion ϵ	1e-3

Table 1 Parameters for de-orbit maneuver

The boundaries for state and control variables are set as:

$$
\begin{aligned}
\mathbf{x}_{min} &= [3,189.07(km),\ -4\pi,\ -\pi,\ -79.05(km/s),\ -79.05(km/s),\ -79.05(km/s),\ 4,000(kg)] \\
\mathbf{x}_{max} &= [12,756.29(km),\ 4\pi,\ \pi,\ 79.05(km/s),\ 79.05(km/s),\ 79.05(km/s),\ 5,000(kg)] \\
\mathbf{u}_{min} &= [-9,000(N),\ -9,000(N),\ -9,000(N),\ 0] \\
\mathbf{u}_{max} &= [9,000(N),\ 9,000(N),\ 9,000(N),\ 9,000]
\end{aligned} \tag{20}
$$

The initial values for the state and control variables are set as:

$$\mathbf{x}_0 = [6,678(km),\ 0.7853,\ 0,\ 0(km/s),\ 7.69(km/s),\ 0.67(km/s),\ 5,000(kg)] \tag{21}$$

Starting from a specific point on the given mission orbit as the initial state, de-orbit trajectories heading towards reentry targets are generated, each defined by specific re-entry locations and times. In this case, a pool of three reentry targets is defined, and the de-orbit trajectory for each case is shown in Fig.3 and summarized in Table 2.

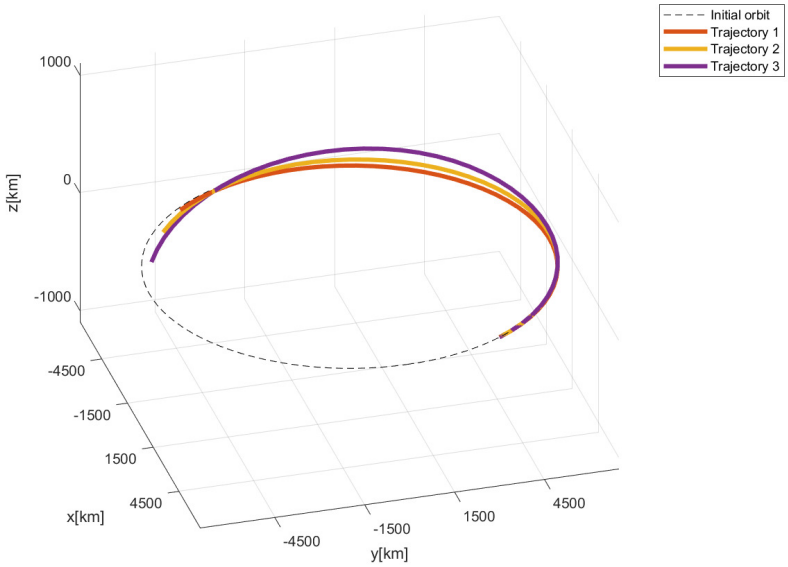

Fig. 3 Synthesized Trajectory plot

The specific results for each reentry target are as follows:

Trajectory	Reentry point (r,θ,ϕ)	Maneuvering time (sec)	Cost	Computation time (sec)
Trajectory 1	(6.4981×10^6, 3.8397, 0)	2.8279×10^3	0.1391	13.34
Trajectory 2	(6.4981×10^6, 4.0142, -0.009)	2.9768×10^3	0.4241	15.88
Trajectory 3	(6.4981×10^6, 4.1887, -0.026)	3.1286×10^3	0.9751	14.93

Table 2 Trajectories data

Based on the result, the reentry target trajectory 1 can be decided as it has the lowest cost. The convergence rate is shown in Fig.4, and the state and control input histories for the trajectory 1-3 are shown in Fig.5 and 6.

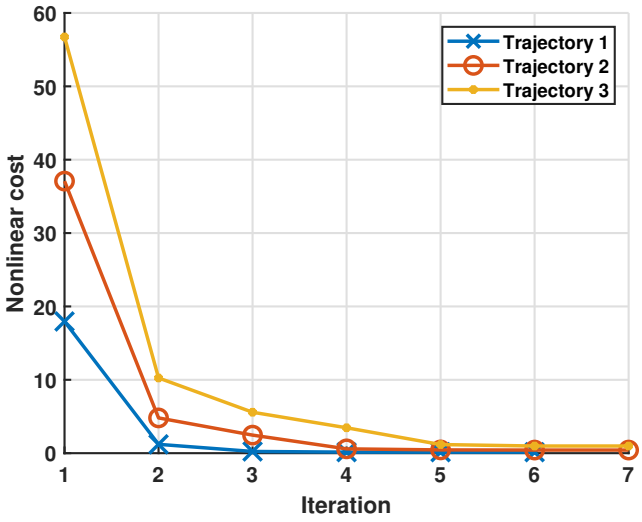

Fig. 4 Convergence profile

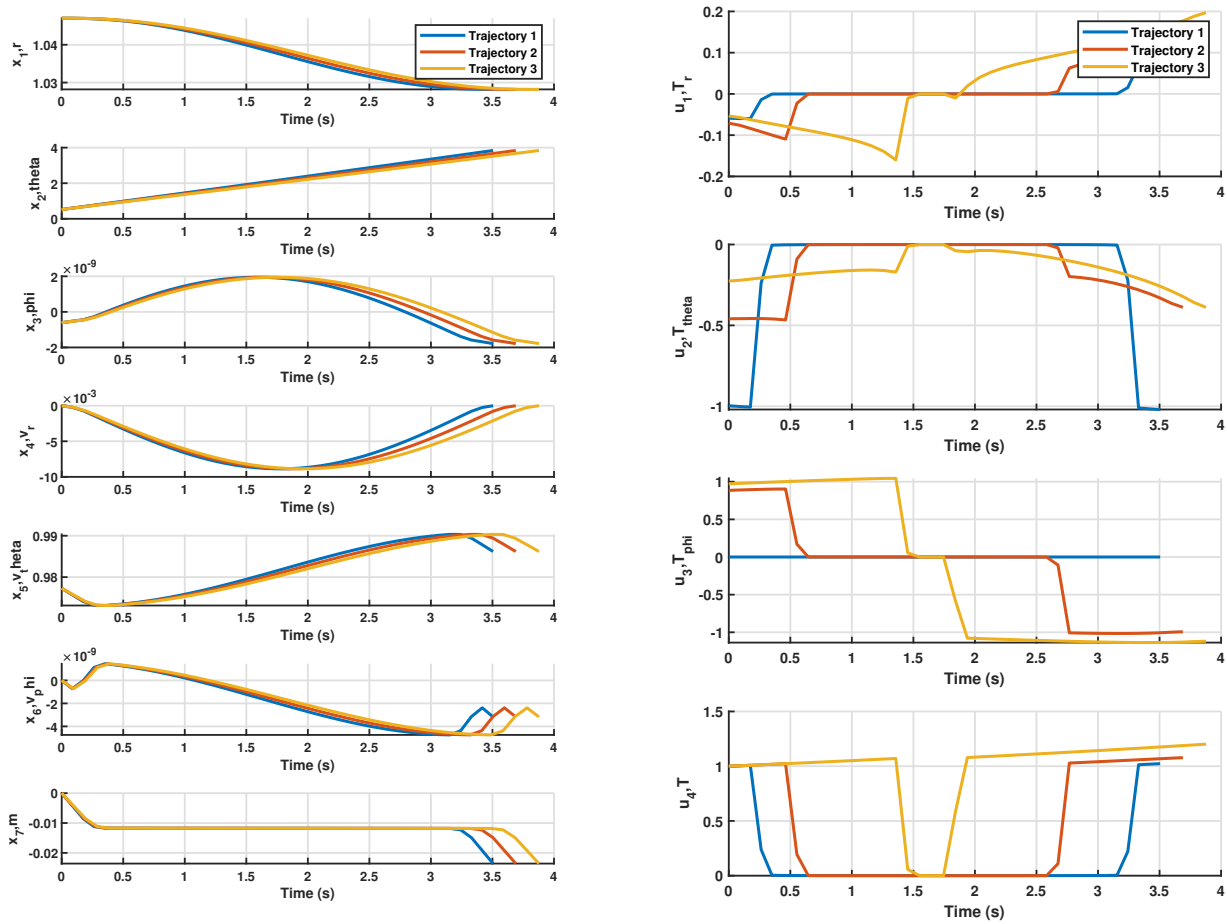

(a) State trajectory **(b) Control trajectory**

Fig. 5 State and control trajectory

As the azimuth angle changes along the trajectory and approaches π, The result becomes similar to the shape of a Hohmann transfer. Also, it can be seen that the cost decreases as the maneuvering time increases. The computation time appears low without meaningful differences, confirming the effectiveness of path calculation using the sequential convex optimization method.

6 Conclusion

A study on the selection of a suitable re-entry target and trajectory after completing a mission has conducted utilizing convex optimization techniques. For de-orbit trajectories, considering the relatively few perturbations and the short time required for maneuvers, the convex optimization allows for the generation of multiple de-orbit paths without significant computation time. By appropriately convexifying the trajectory optimization problem, optimal paths among multiple available re-entry targets can be generated efficiently and reliably.

Appendix

The linearized dynamic system in (15) is defined by A, B, which are given as :

$$A = \frac{\partial \mathbf{f}}{\partial \mathbf{x}} = \begin{bmatrix} 0 & 0 & 0 & 1 & 0 & 0 & 0 \\ -\frac{v_\theta}{r^2\cos\phi} & 0 & \frac{v_\theta \sin\phi}{r\cos^2\phi} & 0 & \frac{1}{r\cos\phi} & 0 & 0 \\ -\frac{v_\phi}{r^2} & 0 & 0 & 0 & 0 & \frac{1}{r} & 0 \\ \frac{2}{r^3} - \frac{v_\theta^2+v_\phi^2}{r^2} & 0 & 0 & 0 & \frac{2v_\theta}{r} & \frac{2v_\phi}{r} & 0 \\ \frac{v_r v_\theta - v_\theta v_\phi \tan\phi}{r^2} & 0 & \frac{v_\theta v_\phi}{r\cos^2\phi} & -\frac{v_\theta}{r} & \frac{v_\phi \tan\phi - v_r}{r} & \frac{v_\theta \tan\phi}{r} & 0 \\ \frac{v_r v_\theta + v_\theta^2 \tan\phi}{r^2} & 0 & -\frac{v_\theta^2}{r\cos^2\phi} & -\frac{v_\phi}{r} & -\frac{2v_\theta \tan\phi}{r} & -\frac{v_r}{r} & 0 \\ 0 & 0 & 0 & 0 & 0 & 0 & 0 \end{bmatrix},$$

$$B = \frac{\partial \mathbf{f}}{\partial \mathbf{u}} = \begin{bmatrix} 0 & 0 & 0 & 0 \\ 0 & 0 & 0 & 0 \\ 0 & 0 & 0 & 0 \\ c & 0 & 0 & 0 \\ 0 & c & 0 & 0 \\ 0 & 0 & c & 0 \\ 0 & 0 & 0 & -\frac{c}{v_e} \end{bmatrix} \tag{22}$$

Acknowledgments

This work was supported by Korea Research Institute for defense Technology planning and advancement(KRIT) grant funded by the Korea government(DAPA(Defense Acquisition Program Administration))(No. KRIT-CT-22-030, ReUSV-41, 2024)

References

[1] Z. Wang. *Trajectory optimization and guidance design by convex programming*. Ph.D. Dissertation, Purdue University, West Lafayette, IN, Aug. 2018.

[2] X. He, X. Zuo, Q. Li, M. Xu, and J. Li. Surrogate-based entire trajectory optimization for full space mission from launch to reentry. *Acta Astronautica*, 190, 2022, pp.83–97. DOI: 10.1016/j.actaastro.2021.09.030.

[3] M.C. Baldwin and P. Lu. Optimal deorbit guidance. *Journal of guidance, control, and dynamics*, 35(1), 2012, pp.93–103. DOI: 10.2514/1.53937.

[4] M. Lin and M. Xu. Entire flight trajectory design for temporary reconnaissance mission. *Transactions of the Japan Society for Aeronautical and Space Sciences*, 60(3), 2017, pp.137–151. DOI: 10.1007/s13272-017-0240-9.

[5] J. Kindler, U. Schoettle, and K. Well. Entry interface window of landing site coober pedy for the experimental vehicle x-38 v201. *Atmospheric Flight Mechanics Conference*, Denver, CO, Aug. 2000.

[6] W.A. Scheel and B.A. Conway. Optimization of very-low-thrust, many-revolution spacecraft trajectories. *Journal of Guidance, Control, and Dynamics*, 17(6), 1994, pp.1185–1192. DOI: 10.2514/3.21331.

[7] D.J. Jezewski and H.L. Rozendaal. An efficient method for calculating optimal free-space n-impulse trajectories. *AIAA journal*, 6(11), 1968, pp.2160–2165. DOI: 10.2514/3.4949.

[8] C.D. Hall and V. Collazo-Perez. Minimum-time orbital phasing maneuvers. *Journal of guidance, control, and dynamics*, 26(6), 2003, pp.934–941. DOI: 10.2514/2.6921.

[9] R.S. Nah, S.R. Vadali, and E. Braden. Fuel-optimal, low-thrust, three-dimensional earth-mars trajectories. *Journal of Guidance, Control, and Dynamics*, 24(6), 2001, pp.1100–1107. DOI: 10.2514/2.4844.

[10] C.A. Kluever. Optimal low-thrust interplanetary trajectories by direct method techniques. *The Journal of the astronautical sciences*, 45, 1997, pp.247–262. DOI: 10.1007/BF03546403.

[11] B. Wall. Shape-based approximation method for low-thrust trajectory optimization. *AIAA/AAS Astrodynamics Specialist Conference*, Honolulu, HI, Aug. 2008.

[12] E. Taheri, I. Kolmanovsky, and E. Atkins. Shaping low-thrust trajectories with thrust-handling feature. *Advances in Space Research*, 61(3), 2018, pp.879–890. DOI: 10.1016/j.asr.2017.11.006.

[13] S. Chien. A generalized timeline representation, services, and interface for automating space mission operations. *SpaceOps 2012 Conference*, Stockholm, Sweden, Jun. 2012.

[14] J. Heiligers, M. Ceriotti, C.R. McInnes, and J.D. Biggs. Displaced geostationary orbit design using hybrid sail propulsion. *Journal of Guidance, Control, and Dynamics*, 34(6), 2011, pp.1852–1866. DOI: 10.2514/1.53807.

[15] A. Saraf, J. Leavitt, M. Ferch, and K. Mease. Landing footprint computation for entry vehicles. *AIAA Guidance, Navigation, and Control Conference*, Providence, RI, Aug. 2004.

[16] Y. Mao, M. Szmuk, X. Xu, and B. Açikmese. Successive convexification: A superlinearly convergent algorithm for non-convex optimal control problems. *arXiv preprint arXiv:1804.06539*, 2018.